Threshold anomaly with weakly bound projectiles: Elastic scattering of ^{9}Be+^{27}Al

P. R. S. Gomes, R. M. Anjos, C. Muri, J. Lubian, and I. Padron
Instituto de Física, Universidade Federal Fluminense, Av. Litoranea s/n, Gragoata, Niterói, R.J., 24210-340, Brazil

L. C. Chamon, R. Liguori Neto, and N. Added
Departamento de Física Nuclear, Universidade de São Paulo, Caixa Postal 66318, 05315-970, São Paulo, S.P., Brazil

J. O. Fernández Niello, G. V. Martí, O. A. Capurro, A. J. Pacheco, J. E. Testoni, and D. Abriola
Laboratorio Tandar, Departamento de Física, Comisión Nacional de Energía Atómica, Av. del Libertador 8250, (1419), Buenos Aires, Argentina

(Received 23 July 2004; published 5 November 2004)

Elastic scattering of the weakly bound ^{9}Be on ^{27}Al was measured at near barrier energies. The optical model data analysis with the real and imaginary parts of a global double-folding potential does not show strong evidence of the usual threshold anomaly. The same result was obtained by using a Woods-Saxon shape optical potential and calculating the potential strengths at the strong absorption radius. The reason for this behavior may be explained by the presence of break-up and/or transfer channels at low energies.

DOI: 10.1103/PhysRevC.70.054605 PACS number(s): 25.70.Bc, 24.10.Ht, 25.70.Mn

I. INTRODUCTION

The elastic scattering of heavy ions at energies near the Coulomb barrier usually shows an anomalous behavior of the energy dependence of the real and imaginary parts of the optical potential, known as the threshold anomaly [1,2]. This anomaly shows up as a localized peak in the real part and the decreasing and vanishing of the imaginary part of the potential in the neighborhood of the Coulomb barrier. It may be ascribed mainly to the coupling of the elastic scattering to other reaction channels. There is a correlation between the real and imaginary parts of the potential due to causality, and consequently they obey the dispersion relation [3].

Therefore, at near barrier energies, when the threshold anomaly is present, nuclear potentials that describe the elastic scattering are no longer slowly energy-dependent, as at high energies. The strong coupling between reaction channels produces an attractive polarization potential ΔV, leading to $V_{\rm eff}=V_o+\Delta V$, where V_o is the unrenormalized folding potential which could be approximated by a phenomenological Woods-Saxon potential obtained by fitting data well above the barrier. If the reaction channels are closed, the strength of the imaginary potential decreases towards zero as the bombarding energy decreases towards the Coulomb barrier.

The situation may be different when one is dealing with weakly bound nuclei. For systems with weakly bound projectiles interacting with heavy targets, there is a strong coupling of the elastic scattering to the break-up process [2,4], which has a larger cross section than the fusion at sub-barrier energies [5–7]. Therefore, it is expected that the threshold anomaly may no longer be present due to the repulsive polarization potential produced by the coupling to the continuum break-up states, which compensates for the attractive polarization arising from couplings to bound states [8–10]. For these nuclei, the rapid decrease of the fusion cross section at sub-barrier energies does not mean that the main reaction channels are closing down at this regime.

Two main approaches are usually used in this kind of study, both describing the elastic scattering in terms of complex optical potentials. One is the use of standard Woods-Saxon energy-dependent optical potentials, with volume ($W_V=W_F$) and surface ($W_S=W_{\rm DR}$) imaginary parts, where the first is responsible for the absorption of flux by the fusion channel, and the second is responsible for the absorption due to direct reaction channels $[W(r,E)=W_F(r,E)+W_{\rm DR}(r,E)]$. In order to minimize the ambiguities of this fit procedure, the potentials are calculated at the strong absorption radius or radius of sensitivity. The alternative approach is the use of double-folding potentials [1], usually with M3Y [11,12] or BDM3Y1 [13] effective interactions, suitable for describing the elastic scattering for a wide range of systems over a broad energy range. In this case, Woods-Saxon potentials are also usually used for the imaginary part. However, when weakly bound nuclei are studied [1,8,12,14–16], the corresponding real part of the folding potential needs to be weakened by about 60% in order to fit the data.

For the ^{6}Li projectile, which has a break-up ($\alpha+d$) threshold energy of 1.48 MeV and no bound excited state below this value, the threshold anomaly is not present in the scattering on ^{208}Pb [8], ^{138}Ba [9], and ^{28}Si [10,16]. On the contrary, the imaginary potential may increase at energies around the Coulomb barrier [8,9], when heavy targets are used. For ^{7}Li, however, the anomaly seems to be present for its scattering on the same targets [8,9,16,17]. Important differences between these two lithium isotopes are the strong deformation of ^{7}Li, the much higher break-up ($\alpha+t$) threshold energy, 2.47 MeV, and one bound excited state at 0.48 MeV. Keeley *et al.* [18,19] suggested that the presence of the anomaly is due to inelastic and transfer channels, when reacting with ^{208}Pb, whereas Lubian *et al.* [20] have shown that the anomaly disappears when only the coupling of the ^{7}Li excited state is considered in the scattering on ^{138}Ba. Recently, the scattering of radioactive ^{8}Li on ^{208}Pb was studied [21,22], and there were no signatures for the presence of the anomaly. ^{8}Li has a threshold break-up energy (^{7}Li+n) of 2.03 MeV, intermediate between those of ^{7}Li and

^{6}Li, a positive Q value for the transfer of one neutron, and the first excited state at 0.98 MeV. The absence of an anomaly for this system is interpreted as due to the large one neutron/break-up channels [22] that remain open below the Coulomb barrier.

For weakly bound ^{9}Be scattering, there are controversial results. The anomaly was not observed for scattering on ^{64}Zn [23,24] and ^{209}Bi [25,26], whereas for ^{208}Pb [27] the analysis of the data shows the presence of the anomaly. In fact, for scattering on ^{64}Zn, the imaginary potential increases at near barrier energies, instead of the usual decrease observed in the scattering of tightly bound nuclei, and the real potential is roughly constant. For the ^{209}Bi target, an anomalous behavior was observed, since the real part of the potential shows a peak as for tightly bound nuclei, whereas the imaginary potential also increases as the energy decreases towards the barrier. Woolliscroft *et al.* [27] argue that the absolute value of the renormalization factor of the folding potential is very sensitive to the accuracy of the densities used, although the qualitative results that they obtain do not change for the different ^{9}Be densities that were tested. ^{9}Be is a strongly deformed Borromean nucleus with a neutron threshold energy of 1.67 MeV and no bound excited state. After the ^{9}Be breaks-up into ^{8}Be$+n$, the ^{8}Be breaks-up into two α particles with a half-life of the order of 10^{-16} s. In order to contribute to this field, we report measurements of the elastic scattering of ^{9}Be on ^{27}Al at near barrier energies.

II. EXPERIMENTAL DETAILS

The experiments were performed at the 8 UD Pelletron accelerator of the University of São Paulo and at the 20 UD accelerator of the TANDAR Laboratory, Buenos Aires. Beams of ^{9}Be were produced from metallic Be at São Paulo and from BeO at Buenos Aires.

At São Paulo, the elastic scattering was measured with the same set of nine surface barrier detectors used in previous work on the investigation of the threshold anomaly in the scattering of weakly [9,20,23,24] and tightly [28,29] bound nuclei. The detectors were placed at 40 cm from the target, with 5° angular separations between two adjacent detectors and a resolution of the order of 350 keV. In front of each detector there was a set of collimators and circular slits for the definition of the solid angles and to avoid slit-scattered particles. The angle determination was made by reading on a goniometer with a precision of 0.5°. A monitor was placed at 20° with the beam direction for normalization purposes. The relative solid angles of the detectors were determined by Rutherford backscattering of ^{9}Be on a thin ^{197}Au backing layer present in the target. The Al target had a thickness of 60 μg/cm^2. Six beam energies were used, within 12 MeV $\leqslant E_{\rm lab} \leqslant$ 35 MeV, and the angular range was $10° \leqslant \theta_{\rm lab} \leqslant 170°$. The Coulomb barrier at the lab is around 11 MeV. The uncertainties in the differential cross-section data vary from 1% to 8%.

At the TANDAR Laboratory, the fusion cross section for this system was measured at high energies [30], using an $E-\Delta E$ telescope consisting of a large ionization chamber followed by a surface barrier detector. The ^{27}Al target had a thickness of 80 μg/cm^2 and a thin (10 μg/cm^2) backing layer of Au was used for normalization purposes. The angular distributions were obtained for five angles in the range $\theta_{\rm lab} = 10°$ to 25°. The Mylar entrance window of the detector was 250 μg/cm^2 thick and the ionizing gas pressure was 25 Torr of P10. The resolution was good enough to separate events differing by one unit of atomic number. In the measurements for energies of 33 MeV, 40 MeV, and 47.5 MeV, the elastic scattering data were also available, and therefore we included the corresponding angular distributions in the present analysis. However, these additional data, in small angular ranges and for energies well above the barrier, do not strongly affect the investigation of the existence of the threshold anomaly.

III. THE SÃO PAULO POTENTIAL

In previous papers [31,32], a systematization of the real and imaginary parts of the optical potential was described, in the framework of an extensive systematization of nuclear densities and with the energy dependence of the bare potential accounted for by a model based on the nonlocal nature of the interaction [33–35]. This parameter-free potential describes very well the elastic scattering of many different systems from sub-barrier energies up to 200 MeV/nucleon. Only the main characteristics of this interaction, called the São Paulo potential, will be described in the following.

The bare interaction V_N is connected with the folding potential V_F through [31,32]

$$V_N(R,E) \approx V_F(R)\exp\left(-\frac{4v^2}{c^2}\right), \tag{1}$$

where c is the speed of light and v is the local relative velocity between the two nuclei,

$$v^2(R,E) = \frac{2}{\mu}[E - V_C(R) - V_N(R,E)], \tag{2}$$

The folding potential is obtained by using the matter distributions of the nuclei, which take into account the finite size of the nucleon, with a zero range approach for $v(r)$. For the Coulomb interaction, V_C, a double sharp cutoff Coulomb potential was used.

In order to obtain a global parameter-free description of the nuclear interaction, a systematization of nuclear densities was developed [31], based on an extensive study involving charge distributions extracted from electron scattering data and theoretical densities calculated through the Dirac-Hartree-Bolgoliubov model. The two-parameter Fermi (2pF) distribution was adopted to describe the nuclear densities. Within this systematization, the matter densities have an average diffuseness value of $a = 0.56$ fm, and the radius of the distribution of a nucleus with A nucleons is well described by [31]

$$R_0 = 1.31A^{1/3} - 0.84 \text{ fm}. \tag{3}$$

The imaginary part of the interaction is assumed to have the same shape as the real part, with one single adjustable parameter N_i related to its strength,

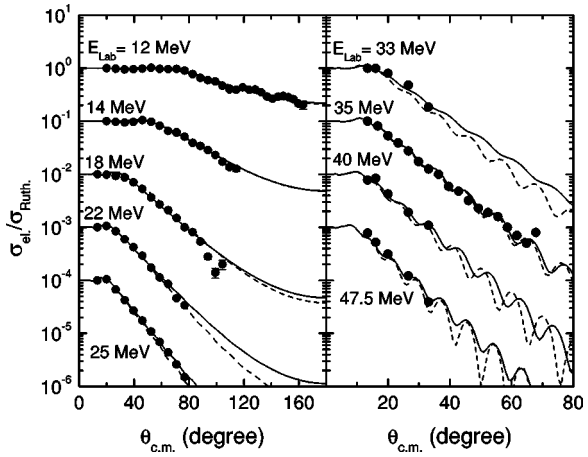

FIG. 1. Elastic angular distributions for the ^{9}Be+^{27}Al systems. The lines correspond to the results obtained with the São Paulo potential, without (dashed lines) free parameters or considering N_i and N_R as free parameters (solid-dashed lines).

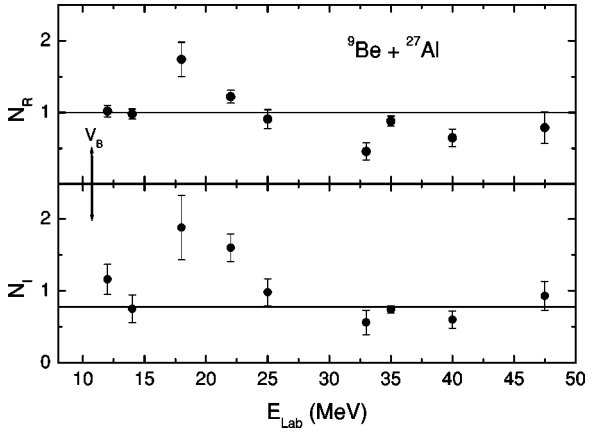

FIG. 2. Energy dependence of the normalization factors N_i and N_R for the real and imaginary parts of the potentials, corresponding to the São Paulo potential. The solid horizontal lines represent the standard values of these parameters.

$$W(R,E) = N_i V_N(R,E). \tag{4}$$

For more than 30 systems, several elastic scattering angular distributions, over wide energy ranges, were simultaneously well fitted with $N_i = 0.78$ [32].

IV. THE DATA ANALYSIS AND RESULTS

In order to explain the elastic scattering angular distributions, the São Paulo potential was used with no free parameter, with densities obtained from the systematization, the strength of the real part [Eq. (1)] multiplied by $N_R = 1.0$, and the strength of the imaginary part equal to the real part multiplied by the value $N_i = 0.78$ [32]. This is the first time that the São Paulo potential is used for the scattering of weakly bound nuclei at energies close to the Coulomb barrier. The results are shown in Fig. 1 with dashed lines. Then, the values of N_R and N_i were considered as free parameters to fit the data. The solid lines in Fig. 1 correspond to the best data fits. The results of the energy dependence of the best N_R and N_i values are shown in Fig. 2. The error bars were calculated as follows: the maximum acceptable χ^2 value was defined as $\chi^2_{\max} = \chi^2_{\min} + \chi^2_{\min}/N$, where N is the number of points of the angular distribution, and the ranges of N_R and N_i should correspond to χ^2 smaller than or equal to $\chi^2_{\max}$. One can observe in Fig. 2 that there are some fluctuations around the standard values $N_R = 1$ and $N_i = 0.78$.

A second approach for the description of the elastic angular distributions was used, considering an optical potential in the form

$$V(r) = -V_0 f(r,R_V,a_V) - iW_{0v} f(r,R_{WV},a_{WV}) - 4iW_{0S}\frac{d}{dr} f(r,R_{WS},a_{WS}) + V_{\mathrm{Coul}}(r), \tag{5}$$

where $f(r,R_i,a_i) = 1/[1+\exp(r-R_i)/a_i]$, $R_i = r_i(A_p^{1/3} + A_t^{1/3})$, $i = V$, WV, WS, and V_0, W_{0V}, and W_{0S} are the real, volume imaginary, and surface imaginary strengths and r_i and a_i their reduced radii and diffusenesses, respectively. $f(r,R_i,a_i)$ is the form factor of the Woods-Saxon potential and V_{Coul} is the Coulomb potential of a uniform charged sphere with radius $R_C = 1.1(A_p^{1/3} + A_t^{1/3})$ fm. A_p and A_t are the projectile and target mass, respectively. The calculations were performed using the ECIS code [36]. In order to avoid a fit procedure with too many free parameters, a χ^2-fit procedure was carried out adjusting just three free parameters: V_0, W_{0S}, and $a_V = a_{WS}$, the last within the range 0.7–0.9 fm. The following values were fixed: $W_{oV} = 15$ MeV, $r_V = r_{WS} = 1.1$ fm, $r_{WV} = 0.9$ fm, $a_{WV} = 0.4$ fm. Very good fits were obtained but, as usual, there are several families of optical potential parameters that describe the angular distributions equally well. As an example, Table I shows one set of parameters that fit the data. In order to reduce the ambiguities, we determined the radii of sensitivity or radii of strong absorption, corresponding to the real and imaginary radii where the different potentials have the same value [9,23,29,30]. The derived mean sensitivity radii were $R_V = 11.3$ fm and $R_W = 8.8$ fm. Figure 3 shows the energy dependence of the potentials at these radii. The error bars represent the range of deviation of the potential corresponding to a χ^2 variation of 1. This approach clearly confirms the results obtained with the São Paulo potential.

TABLE I. Set of optical model parameters that fit the experimental elastic scattering angular distributions.

E_{lab} (MeV)	V_0 (MeV)	W_{0S} (MeV)
12	9.62	4.35
14	10.75	3.76
18	10.48	8.95
22	7.05	8.03
25	5.89	7.81
33	5.9	2.18
35	5.9	5.5
40	4.24	6.09
47	3.75	4.05

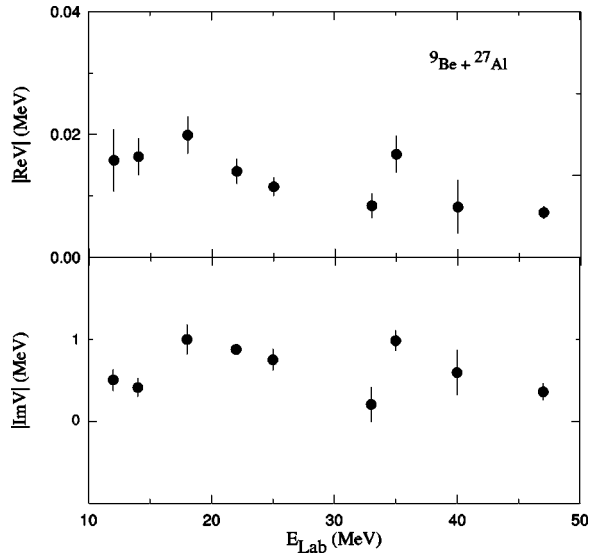

FIG. 3. Energy dependence of the real and imaginary Woods-Saxon optical potential strengths, calculated at the strong absorption radii.

V. DISCUSSION

From both approaches used in the data analysis, the results do not show any strong decrease of the imaginary potential when the energy decreases and approaches the Coulomb barrier, as for systems with tightly bound or ^{7}Li projectiles. On the other hand, one could argue that there is an indication of a bell shape of the real potential and possibly a slight decrease of the imaginary potential at the lowest energies that could be associated with the threshold anomaly. We believe that the most important aspect to be investigated concerning the existence of the threshold anomaly is the behavior of the imaginary potential, since, for the scattering of ^{9}Be on ^{209}Bi [25,26], the bell shape of the real potential is not a signature of the decrease of the imaginary part. We cannot disregard the possibility that the imaginary potential would decrease for energies smaller than the lowest energy that we were able to measure. Even so, we believe that our results show that there are important direct channels still open at energies near the Coulomb barrier for this system, and this is why the imaginary potential does not decrease towards zero at these energies. The two most probable reaction channels for this system are break-up and one neutron stripping. The low threshold energy against the break-up of ^{9}Be leads to the expectation that the cross section for this channel is important even at sub-barrier energies, even though it should not be as large as for heavy targets due to the smaller Coulomb field. In fact, continuum discretized coupled channel calculations have shown that nuclear break-up is important at low energies [37] and experimental data show that break-up has large cross sections at near barrier energies for the medium-light ^{6}Li, ^{9}Be+^{64}Zn systems [38]. The stripping of one neutron has a very large positive Q value, around 6 MeV, and it is also expected to occur at energies close to the barrier.

VI. SUMMARY

The elastic scattering for the ^{9}Be+^{27}Al system at energies near and above the Coulomb barrier was measured. The energy dependence of the real and imaginary parts of the potential was studied by two different approaches: the double-folding São Paulo potential and the Woods-Saxon shape optical potential. Both approaches led to the same conclusion that there is no sharp decrease of the imaginary potential at the lowest energies studied, close to the Coulomb barrier. Therefore, we did not find any significant evidence of the threshold anomaly for this system. The measurement of the elastic scattering at even lower energies should be able to confirm this result. The behavior of the elastic scattering for this system, within the energy range studied, is in agreement with the results obtained for the scattering of ^{9}Be on other targets, and also with the results for the weakly bound ^{6}Li and ^{8}Li projectiles. The reason for the vanishing of the threshold anomaly for these systems is believed to be the strong coupling with the break-up channel, important even at sub-barrier energies, and/or transfer channels with positive Q values. Due to the presence of these reaction mechanisms, with a large cross section at energies close to and below the Coulomb barrier, the imaginary potential does not vanish as the energy decreases towards the Coulomb barrier.

ACKNOWLEDGMENTS

The authors would like to thank the CNPq, CAPES, FAPERJ, FAPESP, and CONICET for their financial support.

[1] G. R. Satchler, Phys. Rep. **199**, 147 (1991).
[2] G. R. Satchler and W. Love, Phys. Rep. **55**, 183 (1979).
[3] M. A. Nagarajan, C. C. Mahaux, and G. R. Satchler, Phys. Rev. Lett. **54**, 1136 (1985).
[4] C. Mahaux, H. Ngo, and G. R. Satchler, Nucl. Phys. **A449**, 354 (1986).
[5] D. J. Hinde *et al.*, Phys. Rev. Lett. **89**, 272701 (2002).
[6] E. F. Aguillera *et al.*, Phys. Rev. C **63**, 061603 (2001).
[7] Y. W. Wu *et al.*, Phys. Rev. C **68**, 044605 (2003).
[8] N. Keeley *et al.*, Nucl. Phys. **A571**, 326 (1994).
[9] A. M. Maciel *et al.*, Phys. Rev. C **59**, 2103 (1999).
[10] A. Pakou *et al.*, Phys. Lett. B **556**, 21 (2003).
[11] G. Bertsh *et al.*, Nucl. Phys. **A284**, 399 (1977).
[12] M. E. Brandan and G. R. Satchler, Phys. Rep. **285**, 143 (1997).
[13] D. T. Khoa *et al.*, Phys. Lett. B **342**, 6 (1995).
[14] Y. Sakuragi, M. Yahiro, and M. Kamimura, Prog. Theor. Phys. **70**, 1047 (1983).
[15] L. Trache *et al.*, Phys. Rev. C **61**, 024612 (2000).
[16] M. A. Tiede, D. E. Trcka, and K. W. Kemper, Phys. Rev. C **44**, 1698 (1991).
[17] A. Pakou *et al.*, Phys. Rev. C **69**, 054602 (2004).
[18] N. Keeley and K. Rusek, Phys. Rev. C **56**, 3421 (1997).
[19] N. Keeley and K. Rusek, Phys. Lett. B **427**, 1 (1998).

[20] J. Lubian *et al.*, Braz. J. Phys. **33**, 323 (2003).
[21] J. J. Kolata *et al.*, Phys. Rev. C **65**, 054616 (2002).
[22] A. Gómez-Camacho and E. F. Aguilera, Nucl. Phys. **A735**, 425 (2004).
[23] S. B. Moraes *et al.*, Phys. Rev. C **61**, 064608 (2000).
[24] P. R. S. Gomes *et al.*, Heavy Ion Phys. **11**, 361 (2000).
[25] C. Signorini, Eur. Phys. J. A **13**, 129 (2002).
[26] C. Signorini *et al.*, Nucl. Phys. **A701**, 23 (2002).
[27] R. J. Wooliscroft *et al.*, Phys. Rev. C **69**, 044612 (2004).
[28] C. Tenreiro *et al.*, Phys. Rev. C **53**, 2870 (1996).
[29] C. Muri *et al.*, Eur. Phys. J. A **1**, 143 (1998).
[30] R. M. Anjos *et al.*, Phys. Lett. B **534**, 45 (2002).
[31] L. C. Chamon *et al.*, Phys. Rev. C **66**, 014610 (2002).
[32] M. A. G. Alvarez *et al.*, Nucl. Phys. **A723**, 93 (2003).
[33] M. A. Candido Ribeiro *et al.*, Phys. Rev. Lett. **78**, 3270 (1997).
[34] L. C. Chamon *et al.*, Phys. Rev. Lett. **79**, 5218 (1997).
[35] L. C. Chamon, D. Pereira, and M. S. Hussein, Phys. Rev. C **58**, 576 (1998).
[36] J. Raynal, Phys. Rev. C **23**, 2571 (1981).
[37] K. Hagino, A. Vitturi, C. H. Dasso, and S. Lenzi, Phys. Rev. C **61**, 037602 (2000).
[38] P. R. S. Gomes *et al.*, Phys. Lett. B **601**, 20 (2004).